Journal of Controlled Release 286 (2018) 425–438

Contents lists available at ScienceDirect

Journal of Controlled Release

journal homepage: www.elsevier.com/locate/jconrel

A facile route to heterotelechelic polymer prodrug nanoparticles for imaging, drug delivery and combination therapy

Daniele Vinciguerra[a], Stéphanie Denis[a], Julie Mougin[a], Merel Jacobs[a], Yohann Guillaneuf[b], Simona Mura[a], Patrick Couvreur[a], Julien Nicolas[a,*]

[a] Institut Galien Paris-Sud, UMR CNRS 8612, Univ Paris-Sud, Faculté de Pharmacie, 5 rue Jean-Baptiste Clément, F-92296 Châtenay-Malabry cedex, France
[b] Aix Marseille Univ, CNRS, Institut de Chimie Radicalaire UMR 7273, campus Saint Jérôme, Avenue Escadrille Normandie-Niemen, 5 Case 542, 13397 Marseille Cedex 20, France

ARTICLE INFO

Keywords:
Polymer
Nanoparticles
Prodrug
Cancer
Combination therapy
Drug delivery

ABSTRACT

A facile and general synthetic methodology has been developed to prepare high drug loading heterotelechelic polymer prodrug nanoparticles; that are nanoparticles obtained by formulation of linear polymers bearing two different molecules at both extremities (at least one of them being a drug). The method relied on the combination of the "*drug-initiated*" method to obtain α-functional polymer prodrugs by nitroxide-mediated polymerization, followed by the nitroxide exchange reaction from a functional nitroxide to install another molecule of interest at the ω chain-end. To validate the proof of concept, two different combinations have been synthesized using polyisoprene (PI) as the polymer building block: one based on gemcitabine and rhodamine (Gem-PI-Rho) for drug delivery and imaging purposes, and one with aminoglutethimide and doxorubicin (Agm-PI-Dox) for combination therapy purposes. Fluorescent polymer prodrug nanoparticles (D_z = 161 nm) were easily obtained by co-nanoprecipitation of Gem-PI and 5 wt% of Gem-PI-Rho. They were observed by confocal microscopy and they also induced significant cytotoxicity on the human breast cancer cell line MCF-7. As for combination therapy purposes, Agm-PI-Dox nanoparticles (D_z = 63–122 nm) led to enhanced cytotoxicity against MCF-7 cells compared to both monofunctional polymer prodrug nanoparticles (ca. 50% decrease in IC_{50} vs. Agm-PI and 65% decrease in IC_{50} vs. PI-Dox) or their equimolar co-nanoprecipitation. This simple and general methodology may pave the way to the design of a broad range of different heterotelechelic polymer prodrug nanoparticles.

1. Introduction

Polymer prodrug nanocarriers are receiving increasing attention as a promising strategy to circumvent the main limitations associated with the traditional encapsulation of drugs into nanoparticulate systems [1, 2]. A chemical linkage between the drug and the polymer scaffold indeed comes with important advantages compared to a simple physical encapsulation, such as: (i) avoiding the "*burst release*" (i.e., the sudden and quick release of a significant amount of drug after administration); (ii) reaching higher drug loadings and (iii) allowing the delivery of drugs that are hardly compatible with the polymer matrix/core.

Polymer prodrug nanocarriers are typically synthesized following three different routes: (i) the "*grafting to*" strategy, which relies on a drug coupling on a preformed polymer; (ii) the "*grafting through*" strategy, consisting in the polymerization of a monomer-bearing drug and (iii) the "*drug-initiated*" approach [3], for which the polymer is grown in a controlled fashion from a drug functionalized by an initiating moiety. The latter method offers significant benefits compared to the two other ones, such as its simplicity (e.g., a few synthetic steps, simpler purification workup, etc.), a quantitative functionalization of the polymer by the drug, adjustable drug loadings (up to ~40 wt %) by fine tuning the polymer chain length and the possibility to be virtually applied to any kind of drug and polymer.

Over the past few years, the versatility and robustness of the "*drug-initiated*" approach was successfully illustrated by its application to many drug/polymer pairs from different polymerization techniques. For instance, ionic ring-opening polymerization (ROP) [4–12] was used to prepare hydrophobic polyester prodrugs nanoparticles based on taxane derivatives, with high drug loadings but that required post-stabilization by PEG-based surfactants to ensure the colloidal stability. Polymer chains were also grown from gemcitabine (Gem), cladribine and paclitaxel by reversible-deactivation radical polymerization (RDRP) techniques; in particular nitroxide-mediated polymerization (NMP) [13–16] and reversible addition-fragmentation chain transfer

* Corresponding author.
E-mail address: julien.nicolas@u-psud.fr (J. Nicolas).

https://doi.org/10.1016/j.jconrel.2018.08.013
Received 22 June 2018; Received in revised form 30 July 2018; Accepted 7 August 2018
Available online 09 August 2018

(RAFT) [15, 17–21] polymerization. These radical polymerization techniques possess great advantages compared to ionic ROP such as mild reaction conditions, great versatility of the polymer structure and composition, the possibility to design well-defined, complex architectures as well as the ease and diversity of polymer functionalization. Interestingly, polymer prodrugs made by RDRP led to surfactant-free nanoparticles with high colloidal stability, drug loadings up to 30 wt% and significant cytotoxicity both in vitro and in vivo.

In the biomedical field, heterotelechelic polymers (i.e., end-functional polymers bearing different reactive end-groups at both chain-ends) are particularly interesting as they offer an opportunity to embed two different biologically active entities at both chain-ends, such as drugs, ligands or imaging agents [22]. However, synthetic strategies to achieve such constructs are generally laborious and not versatile. Also, no example of heterotelechelic polymers bearing two different drugs at the chain ends for combination therapy has ever been reported, which still represents an unmet synthetic challenge. Combination therapy, that relies on the simultaneous administration of two or more drugs, is increasingly used to treat various diseases, including HIV [23, 24], malaria [25, 26] and cancer [27, 28]. Compared to monotherapy, it can overcome some resistance mechanisms, modulate different signaling pathways, maximize the therapeutic effect and even induce a synergy, and reduce adverse effects, which altogether generally lead to better long term prognosis [29, 30]. The development of a facile synthetic route to heterotelechelic polymer prodrug nanoparticles that could be used for drug delivery, imaging or combination therapy purposes would therefore provide the community with new synthetic and therapeutic opportunities.

In this context, we propose a robust and general, yet simple methodology to design highly versatile heterotelechelic polymers for drug delivery applications. The idea is to take advantage of the "*drug-initiated*" method performed by NMP and the high chain-end retention of the controlling agent that offers a robust and flexible post-functionalization opportunity at the ω-chain-end via nitroxide exchange reaction from functional nitroxides (Fig. 1). The efficiency of our approach was illustrated by the design of two very different combinations to validate the proof of concept; one for drug delivery and imaging (i.e., one drug and one imaging probe) and one for combination therapy (i.e., two different drugs). The different heterotelechelic polymer prodrugs will be formulated into the corresponding prodrug nanoparticles and evaluated for their imaging properties by confocal microscopy and cytotoxicity on human breast cancer cells.

2. Materials and methods

2.1. Materials

Gemcitabine (Gem, > 98%), aminoglutethimide (Agm) and doxorubicin·HCl (Dox) were purchased from Carbosynth Limited (UK). Benzotriazol-1-yloxytripyrrolidinophosphonium hexafluorophosphate (PyBOP), *N,N*-diisopropylethylamine (DIPEA), isoprene, 4-(dimethylamino)pyridine (DMAP), succinic anhydride, 4-hydroxy-TEMPO, 1-[bis(dimethylamino)methylene]-1H-1,2,3-triazolo[4,5-*b*]pyridinium 3-oxid hexafluorophosphate (HATU), rhodamine B base (Rho) were purchased from Sigma-Aldrich (France) and used as received. AMA-SG1 [31] and Gem-AMA-SG1 [13] alkoxyamines as well as Rho-piperazine [32] were prepared as reported previously. All other reactants were purchased from Sigma-Aldrich at the highest available purity and used as received. Deuterated chloroform ($CDCl_3$) was obtained from Eurisotop. All other solvents were purchased from Carlo-Erba at the highest grade. Eagle's Minimum Essential Medium (EMEM) and fetal bovine serum (FBS) were purchased from Dulbecco (Invitrogen, France). Penicillin and streptomycin were obtained from Lonza (Verviers, Belgium). LysoTracker Green and Hoechst 33342 were purchased from Life Technologies. *N*-tert-butyl-*N*-(1-diethylphosphono-2,2-dimethylpropyl) nitroxide (SG1, 85%) was kindly supplied by Arkema.

2.2. Analytical methods

2.2.1. Nuclear magnetic resonance spectroscopy (NMR)

NMR spectroscopy was performed in 5 mm diameter tubes in $CDCl_3$ at 25 °C. ^1H and ^{13}C NMR spectroscopy was performed on a Bruker Avance 300 spectrometer at 300 MHz (^1H) or 75 MHz (^{13}C). The chemical shift scale was calibrated based on the internal solvent signals. To characterize nitroxide derivatives, pentafluorophenylhydrazine was added in situ and allowed to react before the analysis [33, 34].

2.2.2. Mass spectrometry

Mass spectra were recorded with a Bruker Esquire-LC instrument. High-resolution mass spectra (ESI) were recorded on an ESI/TOF (LCT, Waters) LC-spectrometer.

2.2.3. Size exclusion chromatography (SEC)

SEC was performed at 30 °C with two columns from Polymer Laboratories (PL-gel MIXED-D; 300 × 7.5 mm; bead diameter 5 mm; linear part 400 to 4×10^5 g·mol^{-1}), a differential refractive index detector (Spectra System RI-150 from Thermo Electron Corp.) and a scanning fluorescence detector (Waters 474). The eluent was chloroform at a flow rate of 1 mL·min^{-1} (Waters 515 pump) and toluene was used as a flow-rate marker. The calibration curve was based on

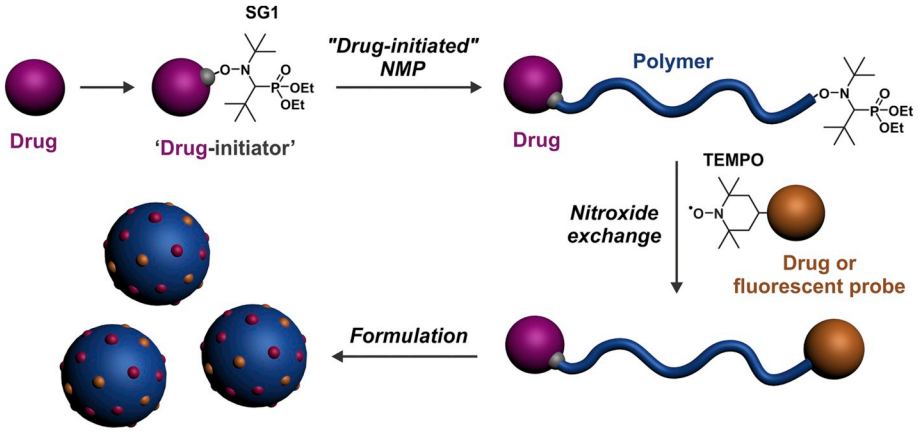

Fig. 1. Synthetic strategy to well-defined, heterotelechelic polymer prodrug nanoparticles for imaging, drug delivery and combination therapy by combining the "*drug-initiated*" method applied to nitroxide-mediated polymerization (NMP) and the nitroxide exchange reaction from a functional nitroxide.

polystyrene (PS) standards (peak molar masses, M_p = 162–523,000 g·mol^{-1}) from Polymer Laboratories. A polyisoprene (PI) calibration curve was constructed by converting the PS standard peak molecular weights (M_{PS}) to PI molecular weights (M_{PI}) using Mark-Houwink-Sakurada (MHS) constants determined for both polymers in CCl_4 at 25 °C. For PI, the MHS constants used were $K_{PI} = 2.44 \times 10^4$ and $\alpha_{PI} = 0.712$. For PS, $K_{PS} = 7.1 \times 10^4$ and $\alpha_{PS} = 0.54$ ($M_w < 16{,}700$ g·mol^{-1}) or $K_{PS} = 1.44 \times 10^4$ and $\alpha_{PS} = 0.713$ ($M_w > 16{,}700$ g·mol^{-1}) [13]. This technique allowed M_n (the number-average molar mass), M_w (the weight-average molar mass), and M_w/M_n (the dispersity, $Đ$) to be determined.

2.2.4. Dynamic light scattering (DLS) and zeta potential

Nanoparticle diameters (*D*z) and zeta potentials (ζ) were measured by dynamic light scattering (DLS) with a Nano ZS from Malvern (173° scattering angle) at a temperature of 25 °C. The surface charge of the nanoparticles was investigated by ζ-potential (mV) measurement at 25 °C after dilution with 1 mM NaCl, using the Smoluchowski equation.

2.2.5. Cryogenic transmission electron microscopy (cryo-TEM)

The morphology of the nanoparticles was observed by cryo-TEM. Briefly, 5 μL of the nanoparticle suspension (0.5 mg·mL^{-1}) was deposited on a Lacey Formvar/carbon 300 mesh copper microscopy grid (Ted Pella). Most of the drop was removed with a blotting filter paper and the residual thin film remaining within the holes was vitrified by plunging into liquid ethane. Samples were then observed using a JEOL 2100HC microscope.

2.2.6. Electronic spin resonance (ESR)

2.2.6.1. Determination of the dissociation rate constant (k_d). ESR experiments were performed on a Bruker EMX 300 spectrometer. The appearance of the nitroxide was followed during the thermolysis of the PI macroalkoxyamine ($[PI]_0 = 1.0 \times 10^{-4}$ M) in *tert*-butylbenzene as solvent (0.6 mL). O_2 was used as radical scavenger. The time evolution of the doubly integrated ESR signal of the TEMPO and SG1 nitroxide radical was followed by ESR spectroscopy at 413 and 385.5 K for 4 h. A first-order fit of the signal allowed the determination of the k_d value. The activation energy E_a was calculated from k_d via the Arrhenius equation with $A = 2.4 \times 10^{14}$ s^{-1} as described elsewhere [32].

2.2.6.2. Determination of the living fraction (LF) of PI-SG1. A PI-SG1 solution ($[PI]_0 = 1.0 \times 10^{-4}$ M) in *tert*-butylbenzene (0.6 mL) was prepared. The residual amount of nitroxide was first determined by ESR using TEMPO solutions as external standards. The solution was then heated up at 393 K for 2 h in open air since O_2 was used as radical scavenger. The solution was then analyzed by ESR and the concentration of the released nitroxide determined using TEMPO solutions as external standards. The living fraction of the polymer chain was then obtained by the difference between the nitroxide concentration after and before thermolysis.

2.2.6.3. Monitoring of the exchange by in situ ESR. A 10^{-3} M pyridine solution of the TEMPO-Rho nitroxide and a Gem-PI-SG1 macroalkoxyamine (1:1 eq) was prepared and inserted into a 3 mm-ESR tube. The tube was degassed for 15 min by argon bubbling. The tube was then inserted into a Bruker EMX 300 spectrometer equipped with a Temperature Control System. The temperature was set to 383 K and the signal was monitored every minute for 16 h.

2.3. Synthesis

2.3.1. Synthesis of Agm-AMA-SG1

Aminoglutethimide (Agm, 0.5 g, 2.15 mmol) was dissolved in 5 mL of dry DMF. PyBOP (1.12 g, 2.15 mmol) and AMA-SG1 (0.790 g, 2.15 mmol) were dissolved in 5 mL of dry DMF in another round-bottomed flask, stirred for 15 min and added by syringe to the first solution. DIPEA (1.11 g, 8.6 mmol) was added dropwise by syringe. The solution was stirred under argon atmosphere for 24 h at room temperature, then diluted with 100 mL EtOAc.The organic phase was washed with 1 M HCl, sat. $NaHCO_3$ aqueous solution, and brine before being dried over $MgSO_4$. The residue was concentrated under reduced pressure and purified by flash chromatography (SiO_2, gradient from Cyclohexane/EtOAc1/1 v/v to EtOAc as eluent) to give 0.86 g of Agm-AMA-SG1 as a white solid. Yield: 69%. ^{1}H NMR ($CDCl_3$, 300 MHz): δ 10.08 (s, 1H, H_a), 8.34 (s, 1H, H_b), 7.80 (d, 2H, H_c), 7.22 (d, 2H, H_c), 4.61 (q, 1H, H_d), 4.11 (m, 4H, H_e), 3.33 (d, 1H, H_f), 2.61–1.90 (m, 6H, H_g), 1.72 (d, 3H, H_h), 1.19 (m, 24H, H_i), 0.86 (t, 3H, H_l). ^{13}C NMR (75 MHz, $CDCl_3$) δ 175.13, 172.26, 171.90, 138.19, 133.49, 126.53, 120.64, 81.85, 69.73, 67.91, 62.50, 61.95, 61.86, 60.28, 60.18, 50.74, 35.61, 32.84, 29.96, 29.32, 28.39, 27.10, 18.95, 16.47, 16.16, 9.02.MS (ESI+): m/z = 604.3 $(M+Na)^+$. Calc. for $C_{29}H_{48}N_3O_7P$: 581.32.

2.3.2. Synthesis of Agm-PI-SG1

Agm-AMA-SG1 (200 mg, 0.344 mmol) was placed in a 15 mL-capacity pressure tube (Ace Glass 8648-164) fitted with plunger valves and thermowells. After addition of isoprene (5.15 mL, 51.6 mmol) and dioxane (5.15 mL), the tube underwent three cycles of freeze-thaw degassing and was then backfilled with argon. The tube was then placed in a preheated oil bath at 115 °C for 4 (**A1**) or 16 h (**A2**) and then cooled down to room temperature by placing it under cold water. The residue was concentrated under reduced pressure and precipitated in cold methanol to give Agm-PI-SG1 as a colorless viscous oil. Another polymerization was performed for 16 h with $[isoprene]_0/[Agm\text{-}AMA\text{-}SG1]_0$ = 300/1 (**A3**). All polymers were characterized by SEC and ^{1}H NMR.

2.3.3. Synthesis of Gem-PI-SG1

A procedure previously published by our group was followed [13]. Briefly, Gem-AMA-SG1 (200 mg, 0.326 mmol) was placed in a 15 mL-capacity pressure tube (Ace Glass 8648–164) fitted with plunger valves and thermowells. After addition of isoprene (6.5 mL, 65.3 mmol) and dioxane (6.5 mL), the tube underwent three cycles of freeze-thaw degassing and was then backfilled with argon. The tube was placed in a preheated oil bath at 115 °C for 8 h (**G2**) or 16 h (**G4, G5**) and then cooled to room temperature by placing it under cold water. The residue was concentrated under reduced pressure and precipitated in cold methanol to give Gem-PI-SG1 as a colorless viscous oil. Other polymerizations were performed for 16 h with $[isoprene]_0/[Gem\text{-}AMA\text{-}SG1]_0$ = 100/1 (**G1, G3**) or $[isoprene]_0/[Gem\text{-}AMA\text{-}SG1]_0$ = 400/1 (**G6**). All polymers were characterized by SEC and ^{1}H NMR.

2.3.4. Synthesis of PI-SG1

AMA-SG1 (100 mg, 0.27 mmol) was placed in a 15 mL-capacity pressure tube (Ace Glass 8648–164) fitted with a plunger valve and thermowell. After addition of isoprene (5.4 mL, 5.4 mmol) and dioxane (5.4 mL), the tube underwent three cycles of freeze-thaw degassing and was then backfilled with argon. The tube was placed in a preheated oil bath at 115 °C for 16 h (**P1**) and then cooled to room temperature by placing it under cold water. The residue was concentrated under reduced pressure and precipitated in cold methanol to give PI-SG1 as a colorless viscous oil. $M_{n,SEC}$ = 2140 g·mol^{-1}, $Đ$ = 1.17.

2.3.5. Synthesis of succinic-TEMPO (4-(1-oxyl-2,2,6,6-tetramethylpiperidin-4-yloxy)-4-oxobutanoic acid)

Succinic-TEMPO was prepared according to published procedure [35]. Briefly, a solution of DMAP (6.38 g, 52.3 mmol) and succinic anhydride (5.23 g, 52.3 mmol) in DCM (30 mL) was added dropwise, at 0 °C and under an argon atmosphere, to a solution of 4-hydroxyTEMPO (3.00 g, 17.4 mmol) in DCM (20 mL). After stirring overnight at room temperature, the solution was quenched with 1 M HCl. The product was extracted three times with DCM. The combined organic layers were washed with brine, dried over $MgSO_4$. After evaporation of the solvent,

succinic-TEMPO was obtained as a white solid. Yield: 98%. ^{1}H NMR ($CDCl_3$, 300 MHz): δ 4.97 (m, 1H), 2.63 (t, 2H), 2.47 (t, 2H), 2.27 (d, 2H), 1.93 (t, 2H), 1.39 (s, 6H), 1.29 (s, 6H).

2.3.6. Synthesis of TEMPO-Rho

DIPEA (1.33 mL, 2 eq) was added by syringe to a solution of HATU (2.2 g, 1.5 eq) and succinic-TEMPO (1.1 g, 1 eq) in DMF (10 mL). After 30 min of stirring, the mixture was added to a solution of Rho-piperazine (2.0 g, 1 eq) and DIPEA (0.66 mL, 1 eq) in DMF (5 mL) and the reaction was stirred at room temperature for 3 h. The mixture was then washed with saturated $NaHCO_3$. The combined organic layers were washed with brine, dried over $MgSO_4$ and concentrated under reduced pression. After purification by flash chromatography (SiO_2, DCM/MeOH 99/1 *v*/v as eluent), 2.0 g of TEMPO-Rho were obtained, as a purple solid. Yield: 68%. ^{1}H NMR ($CDCl_3$, 300 MHz): δ 7.69–6.71 (m, 10H), 5.05 (m, 1H), 3.62 (m, 8H), 3.46 (m, 8H), 2.58 (m, 4H), 1.94 (m, 2H), 1.65 (m, 2H), 1.33 (t, 12H), 1.21 (m, 12H). MS (ESI+): m/z = 765.8 $(M)^+$. Calc. for $C_{45}H_{59}N_5O_6$: 765.45.

2.3.7. Synthesis of TEMPO-Dox

DIPEA (0.64 mL, 2 eq) was added by syringe to a solution of HATU (0.84 g, 1.2 eq) and succinic-TEMPO (0.50 g, 1 eq) in DMF (7 mL). After 30 min of stirring, the mixture was added to a solution of doxorubicin (1.0 g, 1 eq) and DIPEA (0.32 mL, 1 eq) in DMF (3 mL) and the reaction was stirred at room temperature for 3 h. Water was added and then extracted three times with DCM. The combined organic layers were washed with brine, dried over $MgSO_4$ and concentrated under reduced pression. After purification by flash chromatography (SiO_2, DCM/MeOH 98/2 *v*/v as eluent), 0.63 g of TEMPO-Dox were obtained, as a red-orange solid. Yield: 45%. ^{1}H NMR ($CDCl_3$, 300 MHz): δ 8.06 (d, 1H), 7.80 (t, 1H), 7.41 (d, 1H), 6.11 (m, 1H), 5.52 (s, 1H), 5.30 (s, 1H), 5.06 (m, 1H), 4.77 (s, 2H), 4.66 (m, 1H), 4.09 (s, 3H), 3.68 (s, 1H), 3.07–2.90 (m, 2H), 2.75–1.59 (m, 12H), 1.35–1.18 (m, 15H). MS (ESI-): m/z = 796.3 $(M)^-$. Calc. for $C_{40}H_{49}N_2O_{15}$: 797.31.

2.3.8. Synthesis of Gem-PI-Rho (G2R and G3R)

Briefly, 300 mg of Gem-PI (1 eq) and TEMPO-Rho (1 eq) were placed in a 7 mL-vial and dissolved in 1 mL of dry pyridine. After 20 min of degassing under argon, the vial was placed in a preheated oil bath at 110 °C and stirred for 16 h. Gem-PI-Rho was then precipitated two times in cold methanol and dried under reduced pressure until constant weight. The post-functionalization yield was calculated by ^{1}H NMR using the chemical shifts of aromatic protons of Rho (δ = 7.70, 7.55, 7.08 and 6.93–6.67 ppm) and the chemical shifts of aromatic protons and anomeric proton of Gem (δ = 8.26, 7.48 and 6.26 ppm). Functionalization was confirmed by SEC equipped with a fluorescent detector (λ_{ex} = 570 nm, λ_{em} = 595 nm).

2.3.9. Synthesis of Agm-PI-Dox (A1D-A3D)

Briefly, 300 mg of Agm-PI (1 eq) and TEMPO-Dox (1 eq) were placed in a 7 mL-vial and dissolved in 1 mL of dry pyridine. After 20 min of degassing under argon, the vial was placed in a preheated oil bath at 110 °C and stirred for 16 h. Agm-PI-Dox was then precipitated two times in cold methanol and dried under reduced pressure until constant weight. The post-functionalization yield was calculated by ^{1}H NMR using the chemical shifts of aromatic protons of Dox (δ = 8.15, 7.79 and 7.37 ppm) and the chemical shifts of aromatic proton of Agm (δ = 7.53 and 7.23 ppm). The amount of Dox was also determined by UV spectrophotometry at 480 nm (Perkin-Elmer UV/vis spectrophotometer, Germany). Functionalization was confirmed by SEC equipped with a fluorescent detector (λ_{ex} = 480 nm, λ_{em} = 570 nm).

2.3.10. Synthesis of PI-Dox (D1)

Briefly, 300 mg of PI-SG1 (**P1**, 1 eq) and TEMPO-Dox (1 eq) were placed in a 7 mL-vial and dissolved in 1 mL of dry pyridine. After 20 min of degassing under argon, the vial was placed in a preheated oil bath at 110 °C and stirred for 16 h. PI-Dox was then precipitated two times in cold methanol and dried under reduced pressure until constant weight. $M_{n,SEC}$ = 3210 g.mol^{-1}, $Đ$ = 1.22. The amount of doxorubicin was also determined by UV spectrophotometry at 480 nm (Perkin-Elmer UV/vis spectrophotometer, Germany) and was 65%. Functionalization was confirmed by SEC equipped with a fluorescent detector (λ_{ex} = 480 nm, λ_{em} = 570 nm).

2.4. Nanoparticle preparation

Nanoparticles **P1**, **G4, A3**, **A1D-A3D** and **A3coD1** (1:1, mol:mol) were prepared by the nanoprecipitation technique [36]. Briefly, 2.5 mg of the corresponding polymer was dissolved in 0.5 mL of THF and quickly added to 1 mL MilliQ water. THF was evaporated at ambient temperature using a Rotavapor. Intensity-average diameter (D_z) and zeta potential measurements were carried out in triplicate by DLS. Their colloidal stability was assessed in water for 30 days and in cell culture medium supplemented with 10% serum for 13 days. The nanoparticles were kept at 4 °C and allowed to reach room temperature before every measurements.

Gem-PI (**G4**) was also blended and co-nanoprecipitated with 5 wt% of Gem-PI-Rho (**G3R**). Briefly, 0.95 mg of **G4** and 0.05 mg of **G3R** were dissolved in 0.5 mL of THF and quickly added to 1 mL MilliQ water. THF was evaporated at ambient temperature using a Rotavapor. Intensity-average diameter (D_z) and zeta potential measurements were carried out in triplicate by DLS.

2.5. Cell lines and cell culture

MCF-7 human breast cancer cell line was obtained from the American Type Culture Collection (ATCC) and maintained as recommended. Briefly, MCF-7 cells were grown in Eagle's Minimum Essential Medium (EMEM). All media were supplemented with 10% heat-inactivated FBS (56 °C, 30 min), penicillin (100 U mL^{-1}) and streptomycin (100 µg·mL^{-1}), 1% non-essential amino acids (NEAA) and 5 mL glutamine. Cells were maintained in a humid atmosphere at 37 °C with 5% CO_2.

2.6. Confocal microscopy

MCF-7 cells (2×10^5 per well) were cultured on a coverslip in a culture dish for 24 h to achieve ~60% confluence. Cells were then incubated at 37 °C with free Dox or **A3D** at the concentration of 10 µM for 90 min, or **G4coG3R** at the concentration of 5 µM for 90 min. After treatment, the cells were washed with PBS, stained with LysoTracker Green for 30 min, washed again with PBS and stained with Hoechst 33342 for 20 min under the same incubation conditions. The cells were then washed two times with PBS, before addition of medium and imaged by Confocal Laser Scanning Microscopy (CLSM, Leica TCS SP8) with a HC PL APO CS2 (63×/1.40 Oil) oil-immersion objective. The fluorescence was collected in the range of 412–466 m (λ_{ex} = 405 nm, Hoechst 33342), 508–531 nm (λ_{ex} = 504 nm, Lysotracker Green), 558–708 nm (λ_{ex} = 552 nm, **G4coG3R**) and 585–775 nm (λ_{ex} = 470 nm, **A3D**), using a sequential acquisition mode. The pinhole diameter was set at 1.0 Airy unit giving 0.89 µm optical slice thickness. 12 bit numerical images were obtained with Leica SP8 LAS X software (Version 3.1.5, Leica, Germany).

2.7. In vitro anticancer activity

The MTT [3-(4,5-dimethylthiazol-2-yl)-2,5-diphenyl tetrazolium bromide] assay was used to evaluate the cytotoxicity of the different polymer prodrug nanoparticles. Briefly, cells (5×10^3 per well) were seeded in 96-well plates. After an overnight incubation, cells were then exposed to a series of increasing concentrations of polymer prodrugs, control polymers or free drugs for 72 h. Note that for heterobifunctional

polymer prodrug nanoparticles and the co-nanoprecipitation formulation, the concentration refers to the concentration of each drug. 20 μL of MTT solution (5 mg·mL^{-1} in PBS) were then added in each well. Plates were incubated for 1 h at 37 °C followed by removal of the medium and addition of 200 μL of DMSO to each well to dissolve the formazan crystals. Absorbance was measured at 570 nm using a plate reader (Metertech Σ 960, Fisher Bioblock, Illkirch, France). The percentage of surviving cells was calculated as the absorbance ratio of treated to untreated cells. The inhibitory concentration 50% (IC_{50}) of the treatments was determined from the dose-response curve. All experiments were repeated at least two times (6 replicates per condition) to determine means and SDs and the Student's *t*-test was used to determine statistical differences.

3. Results and discussion

3.1. Design rationale

Whereas the synthesis of α-functional polymers by RDRP from corresponding functional initiators is rather straightforward and usually leads to quantitative functionalization, their efficient ω chain-end functionalization is much more challenging. Among the different end-functionalization routes for NMP-derived polymers [37], the nitroxide exchange reaction was selected. This method relies on a thermally-governed substitution of the nitroxide at the ω chain-end of a preformed polymer by a free nitroxide present in the medium. One of the most important advantages of this post-functionalization reaction relies on the absence of any other reactants than the polymer itself and the free nitroxide, which greatly simplifies the purification procedure [38–43]. Moreover, providing experimental conditions are optimized, a small excess of free nitroxide with respect to the polymer is generally enough for a quantitative functionalization. This is for instance the case when the newly formed polymer-nitroxide bond (termed macroalkoxyamine) is less labile than the original one (e.g., by exchanging SG1 by the TEMPO nitroxide [44, 45] or TEMPO by the TMIO nitroxide [43]), thus acting as an efficient driving force.

Combining the "*drug-initiated*" method and the nitroxide exchange with a nitroxide bearing a biologically active moiety thus appeared as an elegant route, to prepare a variety of different heterotelechelic polymers for drug delivery and imaging applications. Moreover, this strategy is rather unexplored for biomedical applications [41], and has never been applied to polymer prodrugs. This general drug delivery platform was built by polymerizing isoprene from a drug-bearing alkoxyamine based on the nitroxide SG1 [13–16], followed by the nitroxide exchange to position a functional TEMPO nitroxide bearing the molecule of interest at the ω chain end. Polyisoprene (PI) was chosen for its degradability [46–49] and biocompatibility [50], resulting from its structural similarity with natural terpenoids such as retinol, vitamin E or squalene, which are all biocompatible compounds. Interestingly, the interest of PI as drug nanocarriers has already been demonstrated both in vitro and in vivo [13–15]. Also, substitution of SG1 by TEMPO through the nitroxide exchange reaction is known to be efficient [44] and should therefore lead to high chain-end functionalization from functional TEMPO derivatives.

To provide the proof of concept, we illustrated our construction approach by the synthesis of two different model combinations: (i) gemcitabine/rhodamine (Gem/Rho) for drug delivery and imaging and (ii) aminoglutethimide/doxorubicin (Agm/Dox) for combination therapy. Gem was selected as an anticancer drug for its activity against a wide range of solid tumors (e.g., colon, lung, pancreatic, breast, bladder and ovarian cancers) [51] and Rho as an imaging probe because it offers a combination of advantageous properties such as a good photostability, a high extinction coefficient, a high quantum yield and an emission wavelength higher than those commonly associated with autofluorescence of cells in vitro [52]. Also, the Rho moiety derived from a tertiary amide to avoid intramolecular cyclization (which would result in a loss of fluorescence) and thus withholding of the fluorescence emission under a broad range of pH [32].

As for the combination therapy, Dox and Agm where selected as anticancer drugs [53–56] because their association was already investigated by grafting them to the backbone of poly(*N*-(2-hydroxypropyl)methacrylamide) (PHPMA), resulting in an enhanced cytotoxicity in vitro [55, 56]. Dox is a leading drug in anticancer therapy, with a proved efficacy against a broad spectrum of solid tumor such as ovary, breast, thyroid, lung and soft tissue sarcomas [57]. Agm is an aromatase inhibitor [58], used as a second line therapy in advanced breast cancer [59].

3.2. Feasibility of the nitroxide exchange reaction

Given the nitroxide exchange reaction has never been performed on PI, we first investigated the feasibility of this reaction by electronic spin resonance (ESR) on a model PI-SG1 (**P1**, synthesized by NMP from the AMA-SG1 alkoxyamine) and free TEMPO to find the best reaction conditions. To do so, the activation energy of PI-TEMPO and PI-SG1 macroalkoxyamines were first determined. It has indeed been shown that the required amount of nitroxide used for the exchange reaction is related to the bond dissociation energy of the precursor and the exchanged (macro)alkoxyamines [43, 44]. Whereas numerous (macro)alkoxyamines based on TEMPO and SG1 have been prepared and their dissociation analyzed by ESR, there is no data for PI-based macroalkoxyamines or model alkyl moieties. The dissociation of PI-SG1 (**P1**) was first monitored at 385.5 K. A k_d value of 8.43 10^{-4} s^{-1} was obtained leading to an activation energy E_a = 128.8 kJ·mol^{-1} (Fig. S1a). This value is relatively close to the PS-SG1 macroalkoxyamine (E_a = 125 kJ·mol^{-1}), which is also an alkoxyamine bearing a secondary alkyl moiety with a relatively low polarity [60]. The dissociation rate constant of a PI end-capped by a TEMPO derivative (**G2R**) was also determined. At 413 K, $k_d = 6.12 \cdot 10^{-4}$ s^{-1}, which corresponds to an activation energy E_a = 139 kJ·mol^{-1}; that is a 10 kJ·mol^{-1} difference with **P1** (Fig. S1b). Such a difference is in good agreement with SG1- and TEMPO-based alkoxyamines bearing other alkyl moieties (8.5 and 11.1 kJ·mol^{-1} difference for the styryl and benzyl moiety, respectively) [37] and similar to the one between PS-SG1 and PS-TEMPO [44].

ESR is also a method of choice to determine the living fraction (LF) of macroalkoxyamines; that is the amount of polymer end-capped by the nitroxide. It was shown that the LF of a nitroxide-terminated polymer is strongly dependent on the polymerization conditions and the molar mass of the polymer [61]. The LF of three Gem-PI-SG1 samples of different molar masses (**G1**, **G5** and **G6**) were measured by ESR (Table 1). As expected the LF values were very high (81–98 mol%) with a nearly quantitative livingness for the lowest M_n, indicating that Gem-PI-SG1 is suitable for the nitroxide exchange from TEMPO derivatives.

Therefore, these preliminary studies on model PI-based macroalkoxyamines successfully established the feasibility of this approach.

3.3. Heterotelechelic polymer prodrug synthesis

For both heterotelechelic polymer prodrugs (i.e., Gem-PI-Rho and Agm-PI-Dox), the drug in α position (i.e., Gem or Agm) was covalently linked to the AMA-SG1 alkoxyamine, followed by NMP of isoprene to yield the corresponding α-functional PI-SG1 prodrugs (Scheme 1 and Scheme 2). They were then subjected to the nitroxide exchange reaction from a functional TEMPO nitroxide bearing either Rho or Dox, to yield the desired heterotelechelic polymer prodrugs.

3.3.1. Synthesis of heterotelechelic polymer prodrugs for drug delivery and imaging (Gem-PI-Rho)

The synthetic route to prepare Gem-PI-Rho prodrugs is presented in Scheme 1. By adjusting the polymerization time or the monomer/initiator molar ratio [13], a small library of Gem-PI (**G1–G6**) of different

Table 1
Characterization of Gem-PI and Gem-PI-Rho Polymer Prodrugs (G = Gem-PI, GR = Gem-PI-Rho).

Prodrug	$M_{n,SEC}$[a] (g·mol^{-1})	$Đ$[a]	$M_{n,NMR}$ (g·mol^{-1})	$DP_{n,NMR}$[d]	Rho/Gem[e]	Drug loading (wt%)[f]	Living fraction (LF, mol.%)[g]
G1	700	1.59	1360[b]	11	–	37.6	98
G2	1320	1.55	2230[b]	24	–	19.9	–
G3	2410	1.30	4170[b]	52	–	10.9	–
G4	2880	1.20	2450[b]	27	–	9.1	–
G5	4750	1.30	4580[b]	58	–	5.5	81
G6	7340	1.20	4180[b]	52	–	3.6	83
G2R	2040	1.26	3000[c]	28	0.95	12.9	–
G3R	2530	1.30	4280[c]	46	0.97	10.4	–

[a] Determined by SEC, calibrated with PS standards and converted into PI by using Mark-Houwink-Sakurada parameters.
[b] Calculated according to $M_{n,NMR} = (DP_{n,NMR} \times MW_{isoprene}) + MW_{alkoxyamine}$.
[c] Calculated according to $M_{n,NMR} = (DP_{n,NMR} \times MW_{isoprene}) + MW_{AMA\text{-}Gem} + MW_{TEMPO\text{-}Rho}$.
[d] Calculated from ratio of areas under the peak at 6.1–6.3, 7.3–7.5, 8.0–8.2 ppm (aromatic and anomeric proton of Gem) and 5.0–5.5 ppm (vinylic H in isoprene repeat unit (1,4-addition), corresponding to ~81% of total isoprene units).
[e] Calculated from ratio of areas under the peak of aromatic protons of Rho at 7.8–7.6, 7.6–7.5, 7.1–7.0, 6.9–6.8 ppm and aromatic and anomeric protons of Gem at 6.1–6.3, 7.3–7.5, 8.0–8.2 ppm.
[f] Calculated according to $MW_{Gem}/M_{n,SEC}$.
[g] Determined by ESR.

molar masses was synthesized by NMP of isoprene from the Gem-bearing alkoxyamine AMA-SG1 (Scheme 1b and Table 1). The resulting polymers exhibited low dispersity ($Đ$ = 1.20–1.59) and high drug loadings up to 38 wt%, which is ~10 times higher than most traditional drug-loaded nanoparticles.

To confer imaging ability to Gem-PI prodrugs by nitroxide

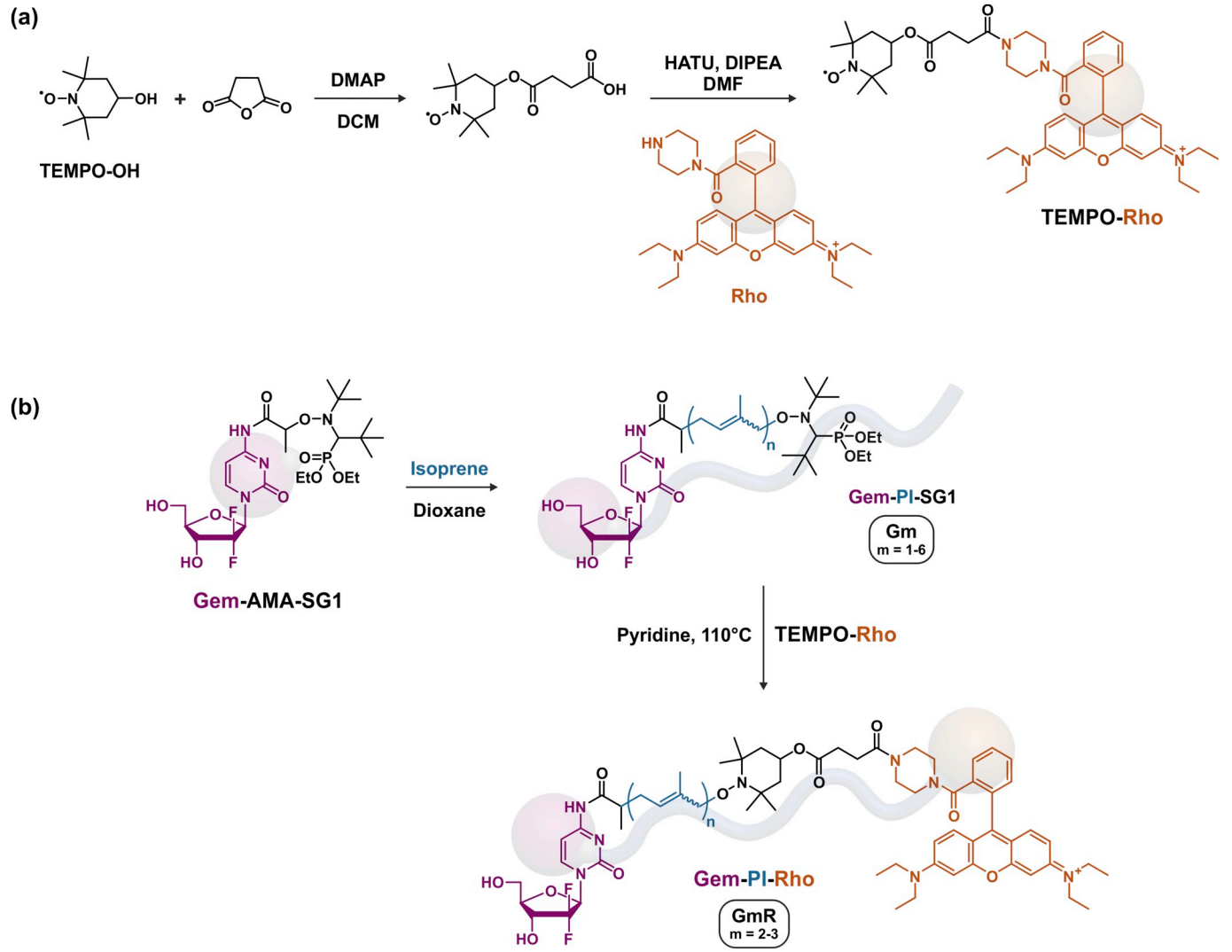

Scheme 1. (a) Synthesis of TEMPO-Rho and (b) heterobifunctional Gem-PI-Rho polymer prodrug by "*drug-initiated*" nitroxide-mediated polymerization (NMP) of isoprene from Gem-AMA-SG1 alkoxyamine followed by nitroxide exchange from TEMPO-Rho. PI = polyisoprene, Gem = gemcitabine and Rho = rhodamine.

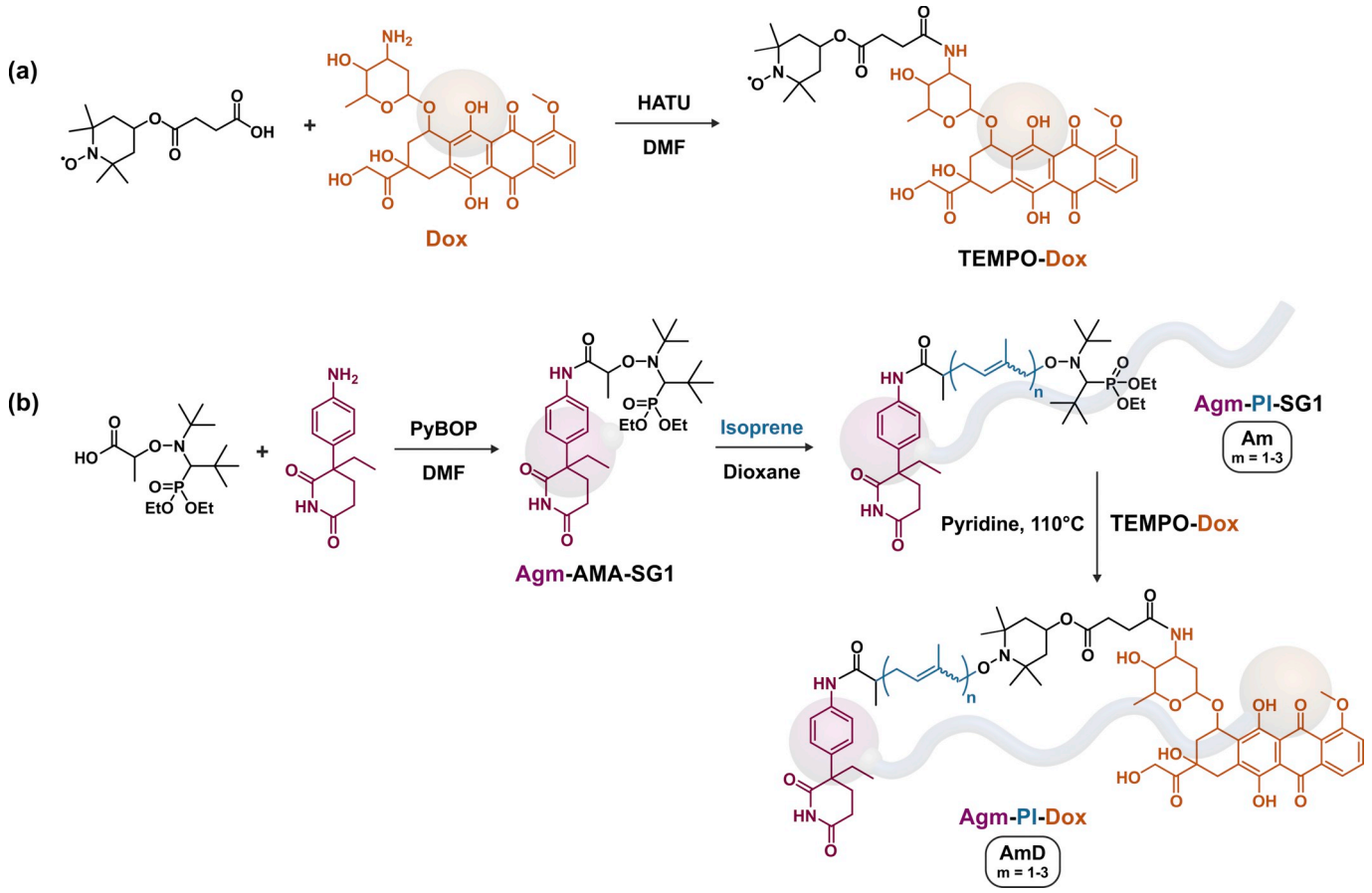

Scheme 2. (a) Synthesis of TEMPO-Dox and (b) heterobifunctional Agm-PI-Dox polymer prodrug by "*drug-initiated*" nitroxide-mediated polymerization (NMP) of isoprene from Agm-AMA-SG1 alkoxyamine followed by nitroxide exchange from TEMPO-Dox. Agm = aminoglutethimide, PI = polyisoprene and Dox = doxorubicin.

exchange, a TEMPO nitroxide functionalized by a Rho moiety was synthesized (Scheme 1a). Hydroxy-TEMPO was reacted with succinic anhydride, while rhodamine B was functionalized with a piperazine ring. TEMPO-Rho was then obtained with a 68% overall yield via amidation using HATU as coupling agent. The nitroxide exchange reaction was then performed in pyridine at 110 °C for 16 h. SEC analysis (DRI detector) of the starting Gem-PI-SG1 (**G2** and **G3**) and the resulting Gem-PI-Rho (**G2R** and **G3R**) did not show any noticeable occurrence of chain termination reaction by recombination (Fig. S2a and S2b). Also, SEC via fluorescence detection confirmed that Gem-PI-SG1 chains have been homogeneously end-capped by TEMPO-Rho moieties as both RI and fluorescence traces of Gem-PI-Rho **G2R** and **G3R** showed the same molar mass distribution profile (Fig. S3).

The presence of TEMPO-Rho at the polymer ω chain-end was first quantitatively measured by ^{1}H NMR (Fig. S4). The NMR spectrum of Gem-PI-Rho (**G3R**) showed the aromatic peaks of Gem and the appearance of protons from Rho in the 4–4.5 ppm region corresponding to the piperazine ring and to protons in α position to the amine, and in the 8–6.5 ppm region corresponding to the aromatic protons of Rho. By comparing the aromatic and anomeric peaks of Gem with the aromatic peaks of Rho, post-functionalization yields for **G2R** and **G3R**, were 95 and 97 mol%, respectively. Moreover, the complete disappearance of the proton signal in the 3.2–3.4 ppm region (proton in α position to the phosphorous atom of SG1) further supported the quantitative chain-end functionalization.

To confirm NMR data, ESR was used to monitor the kinetics of the nitroxide exchange reaction between Gem-PI-SG1 (**G6**) and TEMPO-Rho directly inside the ESR cavity. Because of the high sensibility of the ESR apparatus, the concentration of both reactants was lowered down to 1.0×10^{-3} M, while maintaining an equimolar **G6**:TEMPO-Rho ratio. Since the decomposition is a first order kinetics and the trapping of the macroradical is very fast, influence of the concentration is assumed to be very weak. Note that the exchange reaction has been performed in pyridine for solubility reasons, which is known to increase the rate of dissociation because of its high polarity via stabilization of both the polar transition state and the released nitroxide. According to the literature, the activation energy for the dissociation in polar solvent usually decreases by ~1–3 kJ·mol^{-1}, with a faster decomposition for polar SG1-based compounds than for TEMPO-based counterparts [62].

At the beginning of the reaction, a three-line signal corresponding to the TEMPO nitroxide was overlaid with a small amount of residual SG1 nitroxide, according to the presence of a characteristic six-line signal (Fig. 2a). Upon heating, the intensity of the SG1 nitroxide increased but rapidly decreased because of degradation reactions (Fig. 2a and S5). It has been already shown that in some solvents (e.g., DMF), the SG1 nitroxide is not stable at high temperature [63]. Therefore, the low stability of the SG1 nitroxide in such conditions avoided the direct monitoring of the exchange reaction since the total amount of the free nitroxide was not stable.

Nevertheless, by subtracting the signal of the SG1 nitroxide to the total amount of free nitroxide in the medium, it was possible to determine the evolution with time of the concentration of TEMPO-Rho nitroxide in solution (Fig. S5) and thus the amount of TEMPO-Rho coupled to Gem-PI macroradicals (Fig. 2b). An exponential increase of the desired heterotelechelic Gem-PI-Rho followed by a plateauing of the conversion close to 80% were obtained. Such a value is in line with the LF value determined earlier for Gem-PI-SG1 (**G6**, LF = 83%), showing that the exchange reaction was quantitative under these conditions

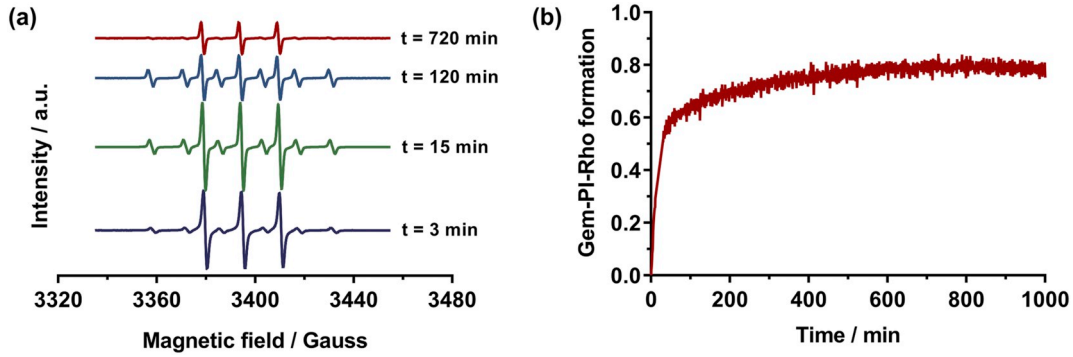

Fig. 2. (a) Monitoring of the nitroxide exchange reaction between Gem-PI-SG1 (**G6**) and TEMPO-Rho (three-line signal refers to TEMPO and six-line signal refers to SG1). (b) Conversion of Gem-PI-SG1 (**G6**) into Gem-PI-TEMPO-Rho.

Table 2
Characterization of Agm-PI, PI-Dox and Agm-PI-Dox polymer prodrugs (A = Agm-PI, AD = Agm-PI-Dox, D = PI-Dox).

Prodrug	$M_{n,SEC}$[a] (g·mol^{-1})	$Đ$[a]	$M_{n,NMR}$ (g·mol^{-1})	$DP_{n,NMR}$[d]	Dox/Agm[e]	Total drug loading (wt%)	Dox[i] (mol.%)
A1	2780	1.22	2610[b]	30	–	8.0[f]	–
A2	3850	1.33	3520[b]	43	–	5.8[f]	–
A3	5100	1.39	7290[b]	99	–	4.4[f]	–
A1D	3370	1.18	3340[c]	33	quant.	23.0[g]	quant.
A2D	4620	1.27	4520[c]	50	95	16.8[g]	quant.
A3D	6500	1.28	7070[c]	88	82	11.9[g]	79.2
D1	3210	1.22	–	–	–	16.9[h]	65.0

[a] Determined by SEC, calibrated with PS standards and converted into PI by using Mark-Houwink-Sakurada parameters.
[b] Calculated according to $M_{n,NMR} = (DP_{n,NMR} \times MW_{isoprene}) + MW_{alkoxyamine}$.
[c] Calculated according to $M_{n,NMR} = (DP_{n,NMR} \times MW_{isoprene}) + MW_{AMA\text{-}Agm} + MW_{TEMPO\text{-}Dox}$.
[d] Calculated from ratio of areas under the peak at 7.20–7.25, 7.50–7.58 ppm (aromatic proton of Agm) and 5.0–5.5 ppm (vinylic H in isoprene repeat unit (1,4-addition), corresponding to ~81% of total isoprene units).
[e] Calculated from ratio of areas under the peak of the aromatic protons of Dox at 8.2–8.1, 7.9–7.7, 7.4–7.3 and aromatic protons of Agm at 7.6–7.5, 7.2–7.1.
[f] Calculated according to $MW_{Agm}/M_{n,SEC}$.
[g] Calculated according to $(MW_{Agm} + MW_{Dox})/M_{n,SEC}$.
[h] Calculated according to $MW_{Dox}/M_{n,SEC}$.
[i] Determined by UV spectroscopy.

Table 3
Characterization Of Gem-PI-Rho Nanoparticles (G = Gem, GR = Gem-PI-Rho).

Prodrug	D_z[a] (nm)	PSD[a]	ζ[a] (mV)	%Gem[b] (wt%)
G4	68	0.134	−29.1	9.1
G4coG3R	161	0.077	12.5	9.3

[a] Measured by dynamic light scattering (DLS) as an average of three different measures.
[b] Calculated according to $MW_{Gem}/(M_{n,SEC(G4)} * 95/100 + M_{n,SEC(G3R)} * 5/100)$.

Table 4
Characterization Of Agm-PI, Agm-PI-Dox And PI-Dox Prodrug Nanoparticles (A = Agm, AD = Agm-PI-Dox, D = Dox).

Prodrug	D_z[a] (nm)	PSD[a]	ζ[a] (mV)	Agm[b] (wt%)	Dox[c] (wt%)
A3	151	0.033	−23	4.4	–
A1D	122	0.096	−43	6.9	16.1
A2D	76	0.126	−39	5.0	11.8
A3D	63	0.100	−31	3.5	8.4
D1	66	0.211	−29	–	16.9
A3coD1	161	0.154	−69	2.8	6.5

[a] Measured by dynamic light scattering (DLS) as an average of three different measures.
[b] Calculated according to $MW_{Agm}/M_{n,SEC}$.
[c] Calculated according to $MW_{Dox}/M_{n,SEC}$.

(i.e., each SG1 nitroxide was replaced by a TEMPO-Rho). It is also worth mentioning that, similarly to the exchange between TMIO and TEMPO nitroxides [43], a 1:1 M ratio between the SG1-terminated polymer and the functional TEMPO was enough to reach a nearly quantitative functionalization, which represents an important advantage over other procedures [44].

ESR was also used to assess the purity of Gem-PI-Rho polymers. They were heated up at 140 °C for 2 h to perform a quantitative release of the nitroxide, whether it is SG1 or TEMPO. Not only ESR analyses did not show any remaining trace of free functional TEMPO before heating, but only TEMPO-related signals were obtained after heating, as a result of a very efficient purification process and a quantitative nitroxide exchange reaction since no SG1 signal was observed (Fig. S6).

3.3.2. Synthesis of heterotelechelic polymer prodrugs for combination therapy (Agm-PI-Dox)

Agm-PI-Dox polymer prodrugs were synthesized following the same synthetic route (Scheme 2).

Agm-AMA-SG1 was prepared via PyBoP coupling between AMA-SG1 and Agm with a 69% yield (Scheme 2b and Fig. S7) and subsequently used to initiate the NMP of isoprene in 1,4-dioxane at 115 °C. A small library of Agm-PI (**A1–A3**) was synthesized and reacted with TEMPO-Dox (previously prepared by coupling hydroxy-TEMPO and Dox by HATU-assisted coupling, see Scheme 2a), to give the corresponding Agm-PI-Dox (**A1D-A3D**, Table 2). These heterobifunctional polymer prodrugs bearing both drugs exhibited variable molar masses and low dispersities ($M_{n,SEC}$ = 3370–6500 g·mol^{-1}, $Đ$ = 1.22–1.39). As with Rho, Dox fluorescence enabled to evaluate the effectiveness of the

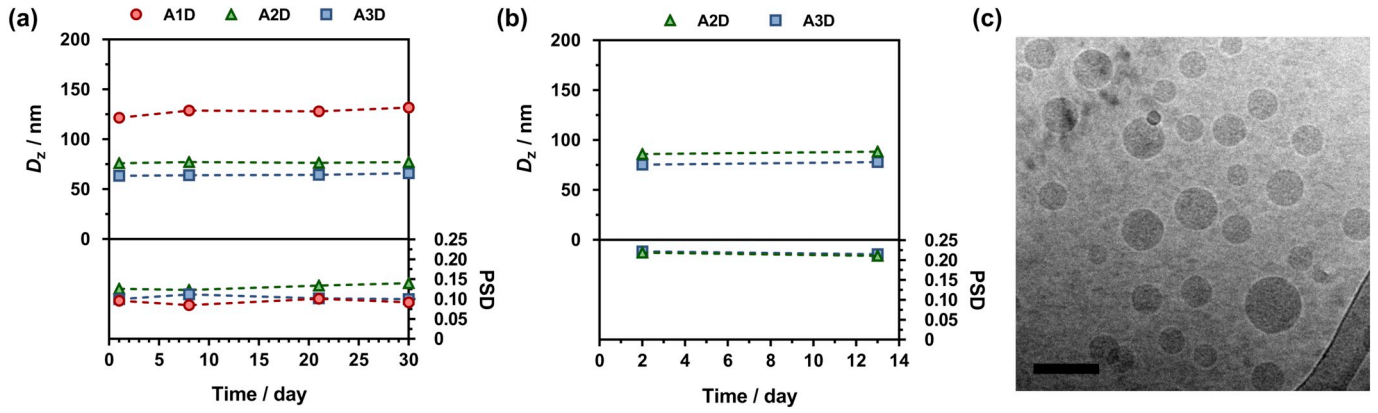

Fig. 3. Evolution of the average diameters (D_z) and the particle size distributions (PSD) measured by DLS of Agm-PI-Dox nanoparticles (**A1D**, **A2D**, **A3D**) in (a) water and (b) cell culture medium (**A2D**, **A3D**). (c) Representative Cryo-TEM image of Agm-PI-Dox nanoparticles **A3D** (scale bar = 100 nm).

nitroxide exchange reaction and the purity of the final polymer by SEC (Fig. S8). The efficiency of the exchange reaction was calculated by ^{1}H NMR by comparing the aromatic proton signals of Dox and Agm (Table 2). It was quantitative for **A1D** (Figs. S9–S10) and as high as ~95% for **A2D**. Here again, the complete disappearance of the proton signal in α position to the SG1 phosphorous atom was observed. However, it was not possible to obtain a reliable measurement of the exchange efficacy by ESR likely because Dox acted as a radical scavenger via its quinone ring. The successful coupling of Dox was also proved by UV spectroscopy based on a calibration curve using free Dox. The amount of Dox coupled to the polymers for **A1D**-**A3D** ranged from 79% to quantitative. The nitroxide exchange reaction was also applied to PI (**P1**) from TEMPO-Dox using optimized experimental conditions reported earlier and yielded PI-Dox (**D1**) as a control monofunctional polymer prodrug (Fig. S11).

All these data indicated a (nearly) quantitative ω-functionalization of "*drug-initiated*" SG1-terminated PI by the nitroxide exchange reaction from TEMPO nitroxides, bearing either a fluorescent probe or another drug, to yield the corresponding well-defined heterotelechelic polymer prodrugs. The general synthetic scheme proved to be simple, yet efficient, with good yields and most importantly very flexible since both chain-ends were readily functionalized with the desired molecule. By combining the quantitative α-functionalization of the "*drug-initiated*" method and the nearly quantitative nitroxide exchange reaction, ~1:1 M ratios between both chain-end moieties were obtained. Note that the nitroxide exchange reaction was conducted to completion to test the robustness of the strategy but it could easily be tuned to target any kind of intermediate ratios simply by playing with the amount of functional TEMPO in the medium during the exchange reaction.

3.4. Nanoparticles formulation and colloidal characteristics

Fluorescent polymer nanoparticles are usually obtained by hydrophobic dye encapsulation during the nanoparticle formulation process. However, strong limitations are often observed including potential leakage of the fluorescent dye out from the nanoparticles, resulting in inaccurate or even wrong interpretations of fluorescence images [64]. Covalent linkage of the fluorescent dye to the polymer nanoparticle is therefore highly desirable. A convenient strategy to fluorescently label "*drug-initiated*" polymer prodrug nanoparticles is to grow a short PI chain from a fluorescent dye and to *co*-nanoprecipitate a small amount of the resulting dye-polymer with a drug-polymer prodrug obtained by the "*drug-initiated*" method, leading to mixed nanoparticles containing both the dye and the drug separately linked to a PI chain. This approach has been illustrated by the co-nanoprecipitation of a few wt% of naphthalimide-PI (Napth-PI) with CdA-PI, leading to mixed nanoparticles suitable for imaging studies by confocal microscopy while still maintaining their cytotoxic activity to cancer cells [16]. However, such a blending strategy always resulted in decrease of the overall drug loading compared to nanoparticles only made from monofunctional drug-polymer conjugates. This issue can be easily overcome by blending heterotelechelic polymer prodrugs comprising both the drug and the imaging agent with the drug-polymer to keep a nearly constant drug loading. We illustrated this strategy by the co-nanoprecipitation of Gem-PI (**G4**) with 5 wt% Gem-PI-Rho (**G3R**), giving fluorescent nanoparticles of 161 nm in average diameter with narrow particle size distribution and the same drug loading as pure Gem-PI nanoparticles **G4** (Table 3). The surface charge of **G4coG3R** nanoparticles increased compared to that of **G4** nanoparticles, as the result of the surface positioning of positively charged Rho moieties.

Heterobifunctional polymer prodrug nanoparticles for combination therapy were obtained by nanoprecipitation of Agm-PI-Dox (**A1D**-**A3D**) at a concentration of 2.5 mg mL^{-1} in water without any surfactant (Table 4). The co-nanoprecipitation of **A3** and **D1** (1:1 mol ratio), leading to Agm-PIcoPI-Dox (**A3coD1**), together with the nanoprecipitation of the corresponding monofunctional polymers Agm-PI (**A3**) and PI-Dox (**D1**), were also performed. The different heterotelechelic polymer prodrug nanoparticle suspensions exhibited average diameters ranging from 63 to 122 nm as measured by DLS, narrow particle size distributions and strongly negative surface charges, that is forerunner of a high colloidal stability (Table 4). Cryo-TEM images of Agm-PI-Dox nanoparticles showed spherical morphologies with average diameters in agreement with DLS data (Fig. 3c).

Importantly, drug loadings of heterotelechelic polymer prodrug nanoparticles (**A1D**-**A3D**) were significantly higher compared to their counterpart obtained by *co*-nanoprecipitation (**A3coD1**) where more polymer was required for the co-nanoprecipitation to keep the same drug ratio, which is an important advantage provided by those materials.

The long term colloidal stability of the different nanoparticles was also assessed over a period of 30 days in water as both the average diameters and the PSD values were constant (Fig. 3a and Fig. S12a).

For Agm-PI-Dox nanoparticles, the higher the M_n, the lower the average diameter and the PSD, in good agreement with literature data on PI-based prodrugs [14]. Interestingly, polymer prodrugs based on Dox led to smaller nanoparticles, which could be explained by π–π interaction between Dox molecules, resulting in denser and thus smaller nanoparticles [65]. These results are in line with UV–Vis spectroscopy measurements, which showed a redshift of the nanoparticle absorbance of about 25 nm, assigned to stacking interactions (Fig. S13) [66, 67]. Importantly, Agm-PI-Dox nanoparticles (**A1D**-**A3D**), Agm-PIcoPI-Dox nanoparticles (**A3coD1**) and their monofunctional counterparts also exhibited great colloidal stability in cell culture medium up to two weeks (Fig. 3b and Fig. S12b).

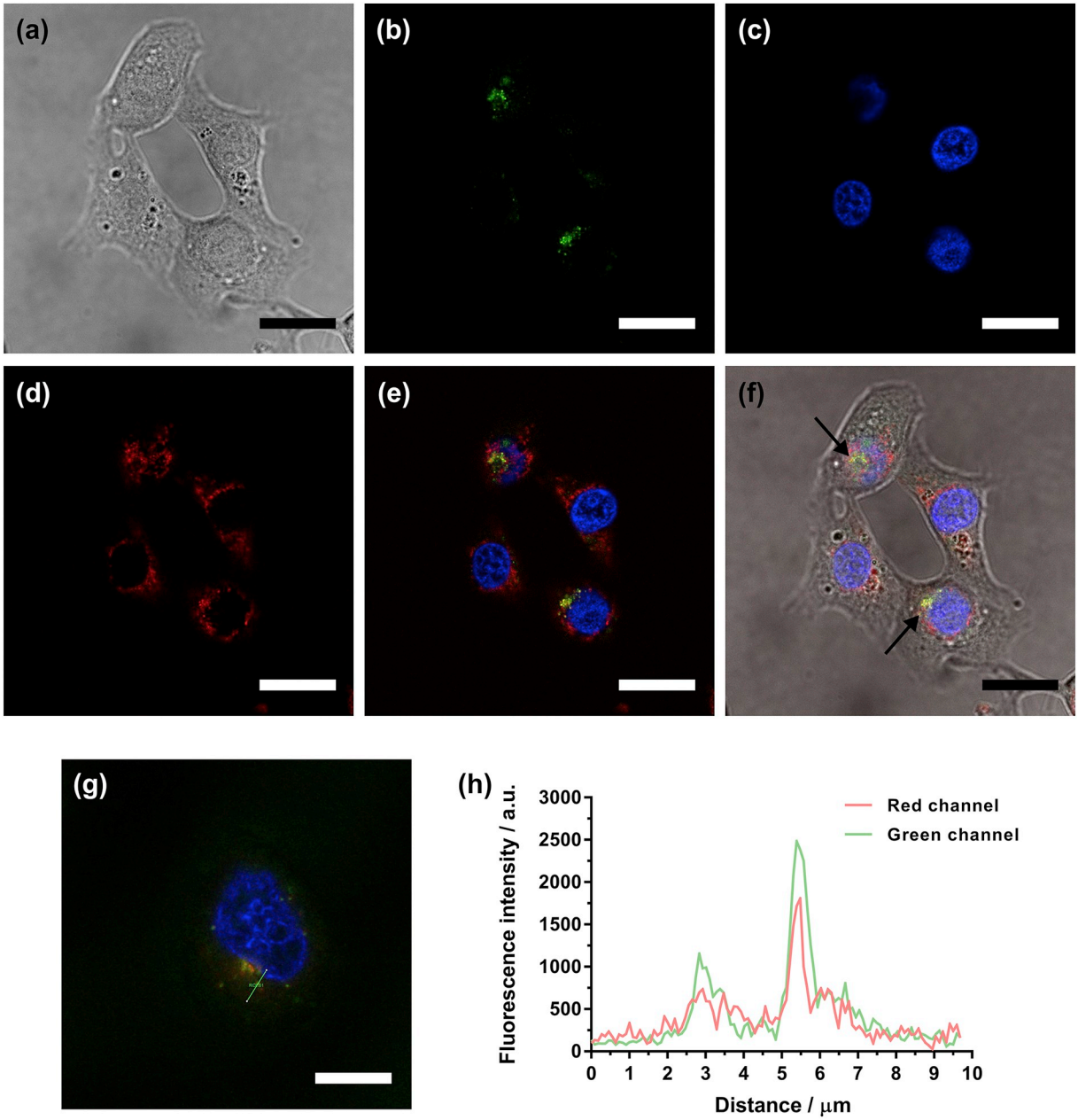

Fig. 4. (a) Nomarski image of MCF-7 cells, (b–d) confocal microscopy images [(b) green (LysoTracker Green), (c) blue (Hoechst 33342) and (d) red (Gem-PI/Gem-PI-Rho **G4coG3R**) channels], (e) merge of green, blue and red fluorescence images, (f) merge of green, blue and red channels with Nomarski image (arrows indicate colocalization), (g) confocal microcopy image (merge of green, blue and red channels) and (h) associated fluorescence intensity profiles. Scale bars = 20 μm. (For interpretation of the references to colour in this figure legend, the reader is referred to the web version of this article.)

3.5. Imaging studies

Confocal microscopy was used to monitor the cellular uptake of Gem-PI/Gem-PI-Rho (**G4coG3R**) nanoparticles by MCF-7 breast cancer cells to assess their subcellular localization. The cells were incubated with **G4coG3R** nanoparticles (red channel) for 90 min and successively with LysoTracker Green (green channel) and Hoechst 33342 (blue channel), for selective staining of the lysosomes and the nucleus, respectively. Gem-PI-Rho nanoparticles proved to be suitable for cell imaging as a strong red fluorescence signal was observed even with a relatively low amount of Rho (i.e., 5 wt% of **G3R**). By overlaying the red, green and blue channels, yellow colocalization spots were observed indicating that Gem-PI-Rho nanoparticles were accumulating into the lysosomes (Fig. 4a–f), which was further supported by analysis of the fluorescence intensity profiles (Fig. 4g and h).

By taking advantage of the inherent fluorescence of Dox, a similar cell imaging experiment was performed with Agm-PI-Dox (**A3D**) nanoparticles. MCF-7 cells were subjected to the same treatment as for **G4coG3R** nanoparticles and CLSM images also revealed a bright, red fluorescence signal inside the cells. By overlaying the red, green and blue channels, yellow colocalization spots were observed, suggesting that **A3D** nanoparticles were in the lysosomes (Fig. 5), conversely to free Dox that was already found in the nucleus after the same time period (Fig. S14). This observation is in agreement with the polymer prodrug concept, whereby the drug needs to get cleaved from the polymer before being pharmacologically active. It therefore resulted in a delayed internalization of Dox in the nucleus from Agm-PI-Dox (**A3D**) nanoparticles conversely to free Dox.

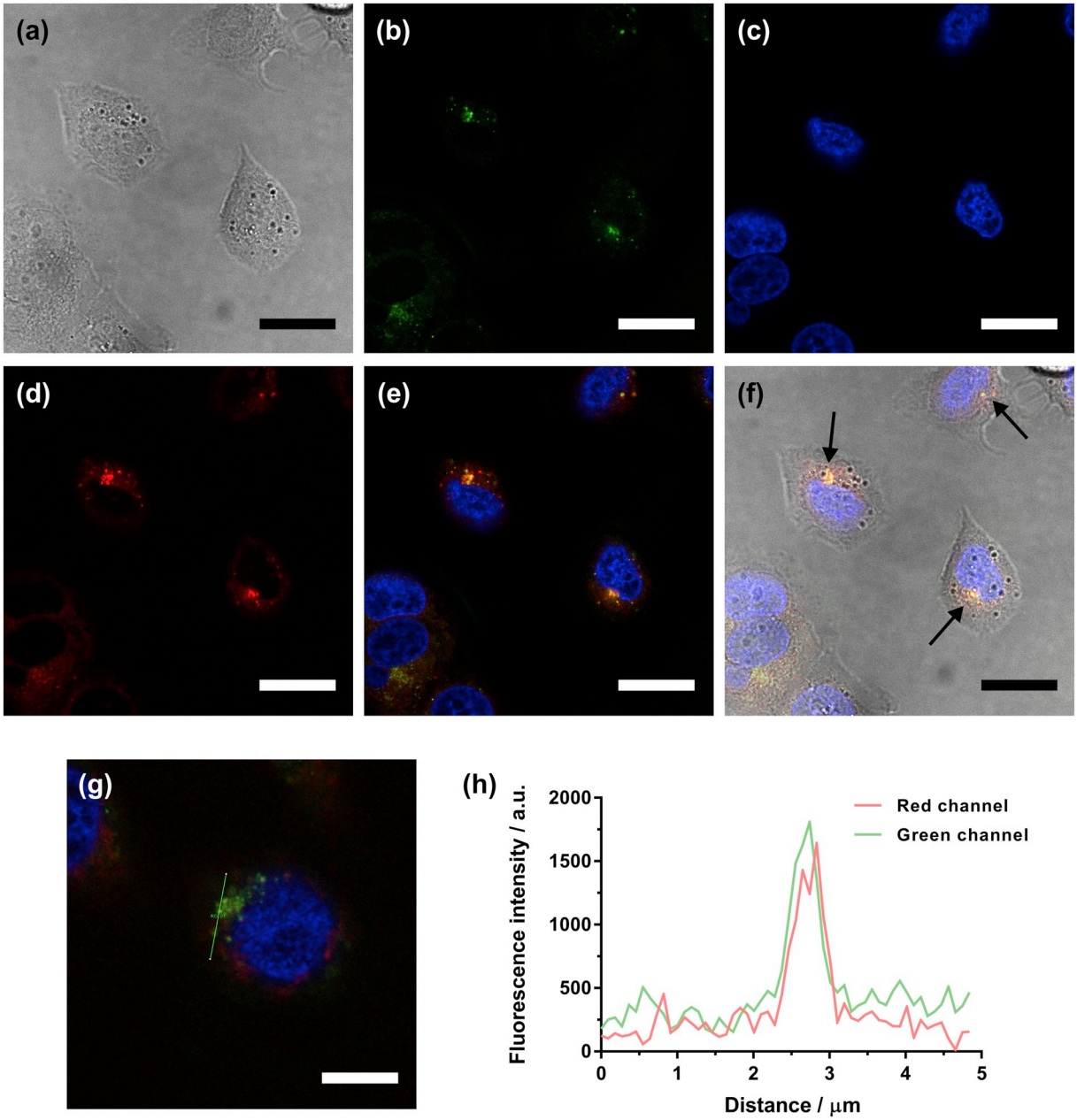

Fig. 5. (a) Nomarski image of MCF-7 cells, (b-d) confocal microscopy images [(b) green (LysoTracker Green), (c) blue (Hoechst 33342) and (d) red (Agm-PI-Dox **A3D**) channels], (e) merge of green, blue and red fluorescence images, (f) merge of green, blue and red channels with Nomarski image (arrows indicate colocalization), (g) confocal microcopy image (merge of green, blue and red channels) and (h) associated fluorescence intensity profiles. Scale bars = 20 μm. (For interpretation of the references to colour in this figure legend, the reader is referred to the web version of this article.)

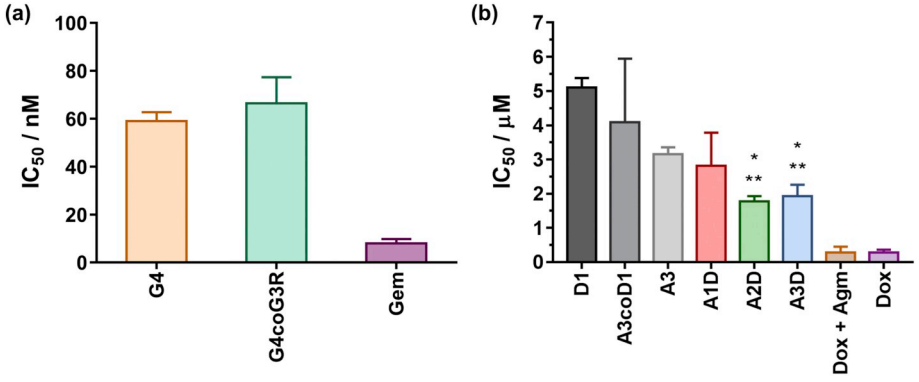

Fig. 6. (a) IC_{50} values ± SD of Gem-PI (**G4**), Gem-PI (**G4**)/Gem-PI-Rho (**G3R**, 5 wt%) and free Gem on MCF-7 cells after incubation of 72 h. (b) IC_{50} values ± SD of Agm-PI-Dox (**A1D-A3D**), Agm-PI (**A3**), PI-Dox (**D1**), Agm-PIcoPI-Dox (**A3coD1**) nanoparticles and free drugs determined by MTT test on MCF-7 cells after 72 h of incubation (**$p < .01$ vs. **D1**, *$p < .05$ vs. **A3**).

Overall, both Gem-PI-Rho and Agm-PI-Dox prodrug nanoparticles proved to be suitable for cellular imaging, with fluorescence signals originating from a dedicated fluorescent probe attached to the polymer chain-end or directly from a fluorescent drug.

3.6. In vitro cytotoxicity

A cytotoxicity study was first performed with Gem-PI/Gem-PI-Rho nanoparticles (**G4coG3R**) on the human breast cancer cell line MCF-7. The cells were incubated for 72 h with increasing concentrations of **G4**, **G4coG3R** or free Gem to determine IC_{50} values. **G4coG3R** nanoparticles showed a similar cytotoxicity profile than that of pure Gem-PI nanoparticles (**G4**), with IC_{50} = 65 μM (Figs. 6a and Fig. S15), showing that fluorescent labeling by chain-end functionalization did not interfere with the cytotoxicity profile. As expected, free Gem exhibited a lower IC_{50} value of 6 nM because of the prodrug nature of **G4** and **G3R**.

The in vitro cytotoxicity of Agm-PI-Dox nanoparticles and their monofunctional counterparts was then investigated on MCF-7 cells under identical experimental conditions. The IC_{50} values were compared to those of the free drugs (alone or in association). Whereas neither PI nanoparticles (**P1**) nor free Agm were cytotoxic at these concentrations (no IC_{50} values could be measured), as previously observed [13–15, 55, 56, 68] (Fig. S16), free Dox led to an IC_{50} value of 0.29 μM, similarly to the 1:1 (mol:mol) physical mixture of free Dox and Agm (Fig. 6b and Fig. S17). Coupling Agm to PI resulted in a drastic increase of the cytotoxicity as PI-Agm prodrug nanoparticles (**A3**) gave an IC_{50} of 3.16 μM, which could be explained by an efficient internalization of the nanoparticles and/or protection from early metabolism [69, 70]. Conversely, PI-Dox (**D1**) nanoparticles showed a reduced cytotoxicity compared to free Dox with an IC_{50} of 5.1 μM, as commonly seen for prodrugs because the drug must be released from the promoiety before recovering its activity.

Very importantly, heterobifunctional Agm-PI-Dox nanoparticle (**A1D–A3D**) showed lower IC_{50} values than monofunctional Agm-PI or PI-Dox nanoparticles, which induced the highest cytotoxicity deriving from the dual functionalization (Fig. 6b and Fig. S17). Moreover, they were also more active than the *co*-nanoprecipitation of both monofunctional polymers at the same molar ratio (**A3coD1**). These results are in good agreement with literature data showing that having both drugs linked to the same polymeric backbone resulted in enhanced cytotoxicity [55, 56].

Also, the higher the M_n of PI for Agm-PI-Dox nanoparticle (**A1D-A3D**), the higher the cytotoxicity, as already observed for monofunctional "*drug-initiated*" polymer prodrug nanoparticles [19]. This trend may be assigned to an enhanced internalization into cancer cells related to the surface hydrophobicity of the nanoparticles and/or their colloidal properties (a lower average diameter is observed when the M_n is increased). Agm-PI-Dox nanoparticle **A1D** with the lowest M_n gave an IC_{50} of 2.82 μM, close to Agm-PI (**A3**), while IC_{50} values of higher M_n Agm-PI-Dox nanoparticle **A2D** and **A3D** were in the 1.8–1.9 μM range. It represents a ~50% decrease in IC_{50} compared to Agm-PI nanoparticles (**A3**) and ~65% compared to PI-Dox nanoparticles (**D1**). Interestingly, the same beneficial effect is not present when Dox and Agm are combined as free drugs, leading a similar IC_{50} value than that of free Dox (0.28 vs. 0.29 μM, respectively). The Combination Index (CI), which is recognized as the standard measure of combination effect [71], indicated an additive effect for **A3D** (CI = 0.98) and a slightly synergistic effect for **A2D** (CI = 0.91), whereas **A3coD1** led to a lesser effect than the expected additive effect (CI = 2.1).

4. Conclusion

By combining the "*drug-initiated*" method and the nitroxide exchange reaction from functional nitroxides, we developed a general approach to design heterotelechelic polymer prodrug nanoparticles, with drug loading up to 23 wt%, for application in drug delivery, imaging and combination therapy. This novel approach is: (i) simple as it only requires a few synthetic steps and only the α-functional polymer and the functional nitroxide are required (i.e., no catalyst or other reagents) which simplifies the purification procedure and leads to high yields; (ii) efficient and robust as (nearly) quantitative chain-end functionalizations are obtained and (iii) versatile as it is applicable to a broad range of different biologically active molecules (e.g., drug, dyes).

In the context of this study, the proof of concept was validated by the synthesis of two different combinations: one with Gem and Rho for drug delivery and imaging, and one with Agm and Dox for combination therapy. Whereas Gem and Rho induced significant cytotoxicity to cancer cells and efficient fluorescent labeling, respectively, combining Agm and Dox led to enhanced cytotoxicity compared to monofunctional polymer prodrug nanoparticle counterparts or their co-nanoprecipitation. Note that the goal of this study was not to find the best drug ratio and/or combination for optimized cytotoxicity, but rather to prove the versatility of this approach by the coupling of three different anticancer drugs and one fluorescent dye.

Another advantage of this approach would be the possibility to finetune the ratio between the two molecules of interest simply by adjusting the stoichiometry of the reactants. This is especially of great interest in the context of combination therapy where any ratio between the two drugs can be obtained.

Overall, the facile development of heterotelechelic polymer prodrug nanoparticles could provide the community with new synthetic and therapeutic opportunities as numerous drug combination for combination therapy can be explored.

Acknowledgement

This work was supported by the European Union's Horizon 2020 research and innovation programme under Marie Skłodowska Curie grant agreement no. 642028 (NABBA). The authors thank Valérie Nicolas (Institut Paris-Sud d'Innovation Therapeutique (IPSIT), Université Paris-Sud) for technical assistance in confocal microscopy, the Service de Microscopie Electronique (UFR de Biologie Intégrative, Université Paris-Sud) for Cryo-TEM analyses and Stéphanie Nicolaÿ for mass spectrometry analyses (Service d'Analyses des Médicaments et Métabolites (Institut Paris-Sud d'Innovation Therapeutique (IPSIT), Université Paris-Sud). Arkema is warmly acknowledged for kindly providing the SG1 nitroxide. CNRS and Université Paris-Sud are also acknowledged for financial support.

Appendix A. Supplementary data

Supplementary data to this article can be found online at https://doi.org/10.1016/j.jconrel.2018.08.013.

References

[1] V. Delplace, P. Couvreur, J. Nicolas, Recent trends in the design of anticancer polymer prodrug nanocarriers, Polym. Chem. 5 (2014) 1529–1544.
[2] F. Kratz, I.A. Müller, C. Ryppa, A. Warnecke, Prodrug strategies in anticancer chemotherapy, ChemMedChem 3 (2008) 20–53.
[3] J. Nicolas, Drug-initiated synthesis of polymer prodrugs: combining simplicity and efficacy in drug delivery, Chem. Mater. 28 (2016) 1591–1606.
[4] R. Tong, J. Cheng, Paclitaxel-initiated, controlled polymerization of lactide for the formulation of polymeric nanoparticulate delivery vehicles, Angew. Chem. 120 (2008) 4908–4912.
[5] R. Tong, J. Cheng, Ring-opening polymerization-mediated controlled formulation of polylactide− drug nanoparticles, J. Am. Chem. Soc. 131 (2009) 4744–4754.
[6] R. Tong, J. Cheng, Drug-initiated, controlled ring-opening polymerization for the synthesis of polymer–drug conjugates, Macromolecules 45 (2012) 2225–2232.
[7] R. Tong, L. Yala, T.M. Fan, J. Cheng, The formulation of aptamer-coated paclitaxel–polylactide nanoconjugates and their targeting to cancer cells, Biomaterials 31 (2010) 3043–3053.
[8] R. Tong, J. Cheng, Controlled synthesis of camptothecin− polylactide conjugates and nanoconjugates, Bioconjug. Chem. 21 (2009) 111–121.
[9] Q. Yin, R. Tong, Y. Xu, K. Baek, L.W. Dobrucki, T.M. Fan, J. Cheng, Drug-initiated ring-opening polymerization of O-carboxyanhydrides for the preparation of

anticancer drug–poly (O-carboxyanhydride) nanoconjugates, Biomacromolecules 14 (2013) 920–929.
[10] J. Azzi, L. Tang, R. Moore, R. Tong, N. El Haddad, T. Akiyoshi, B. Mfarrej, S. Yang, M. Jurewicz, T. Ichimura, Polylactide-cyclosporin A nanoparticles for targeted immunosuppression, FASEB J. 24 (2010) 3927–3938.
[11] S. Aryal, C.-M.J. Hu, L. Zhang, Polymeric nanoparticles with precise ratiometric control over drug loading for combination therapy, Mol. Pharm. 8 (2011) 1401–1407.
[12] J.M. Chan, L. Zhang, R. Tong, D. Ghosh, W. Gao, G. Liao, K.P. Yuet, D. Gray, J.-W. Rhee, J. Cheng, Spatiotemporal controlled delivery of nanoparticles to injured vasculature, Proc. Natl. Acad. Sci. 107 (2010) 2213–2218.
[13] S. Harrisson, J. Nicolas, A. Maksimenko, D.T. Bui, J. Mougin, P. Couvreur, Nanoparticles with in vivo anticancer activity from polymer prodrug amphiphiles prepared by living radical polymerization, Angew. Chem. Int. Ed. 52 (2013) 1678–1682.
[14] Y. Bao, T. Boissenot, E. Guégain, D. Desmaële, S. Mura, P. Couvreur, J. Nicolas, Simple synthesis of cladribine-based anticancer polymer prodrug nanoparticles with tunable drug delivery properties, Chem. Mater. 28 (2016) 6266–6275.
[15] Y. Bao, E. Guégain, J. Mougin, J. Nicolas, Self-stabilized, hydrophobic or PEGylated paclitaxel polymer prodrug nanoparticles for cancer therapy, Polym. Chem. 51 (2018) 724–736.
[16] Y. Bao, E. Guégain, V. Nicolas, J. Nicolas, Fluorescent polymer prodrug nanoparticles with aggregation-induced emission (AIE) properties from nitroxide-mediated polymerization, Chem. Commun. 53 (2017) 4489–4492.
[17] D. Trung Bui, A. Maksimenko, D. Desmaële, S. Harrisson, C. Vauthier, P. Couvreur, J. Nicolas, Polymer prodrug nanoparticles based on naturally occurring isoprenoid for anticancer therapy, Biomacromolecules 14 (2013) 2837–2847.
[18] A. Maksimenko, D.T. Bui, D. Desmaële, P. Couvreur, J. Nicolas, Significant tumor growth inhibition from naturally occurring lipid-containing polymer prodrug nanoparticles obtained by the drug-initiated method, Chem. Mater. 26 (2014) 3606–3609.
[19] Y. Bao, J. Nicolas, Structure–cytotoxicity relationship of drug-initiated polymer prodrug nanoparticles, Polym. Chem. 8 (2017) 5174–5184.
[20] B. Louage, L. Nuhn, M.D. Risseeuw, N. Vanparijs, R. De Coen, I. Karalic, S. Van Calenbergh, B.G. De Geest, Well-defined polymer–paclitaxel prodrugs by a grafting-from-drug approach, Angew. Chem. Int. Ed. 55 (2016) 11791–11796.
[21] B. Louage, M.J. Van Steenbergen, L. Nuhn, M.D. Risseeuw, I. Karalic, J. Winne, S. Van Calenbergh, W.E. Hennink, B.G. De Geest, Micellar paclitaxel-initiated RAFT polymer conjugates with acid-sensitive behavior, ACS Macro Lett. 6 (2017) 272–276.
[22] D. Vinciguerra, J. Tran, J. Nicolas, Telechelic polymers from reversible-deactivation radical polymerization for biomedical applications, Chem. Commun. 54 (2018) 228–240.
[23] A.S. Perelson, P. Essunger, Y. Cao, M. Vesanen, A. Hurley, K. Saksela, M. Markowitz, D.D. Ho, Decay characteristics of HIV-1-infected compartments during combination therapy, Nature 387 (1997) 188.
[24] M. Egger, B. Hirschel, P. Francioli, P. Sudre, M. Wirz, M. Flepp, M. Rickenbach, R. Malinverni, P. Vernazza, M. Battegay, Impact of new antiretroviral combination therapies in HIV infected patients in Switzerland: prospective multicentre study, BMJ 315 (1997) 1194–1199.
[25] R.T. Eastman, D.A. Fidock, Artemisinin-based combination therapies: a vital tool in efforts to eliminate malaria, Nat. Rev. Microbiol. 7 (2009) 864.
[26] F. Nosten, P. Brasseur, Combination therapy for malaria, Drugs 62 (2002) 1315–1329.
[27] B. Al-Lazikani, U. Banerji, P. Workman, Combinatorial drug therapy for cancer in the post-genomic era, Nat. Biotechnol. 30 (2012) 679.
[28] C.-M.J. Hu, L. Zhang, Nanoparticle-based combination therapy toward overcoming drug resistance in cancer, Biochem. Pharmacol. 83 (2012) 1104–1111.
[29] F. Greco, M.J. Vicent, Combination therapy: opportunities and challenges for polymer–drug conjugates as anticancer nanomedicines, Adv. Drug Deliv. Rev. 61 (2009) 1203–1213.
[30] P. Parhi, C. Mohanty, S.K. Sahoo, Nanotechnology-based combinational drug delivery: an emerging approach for cancer therapy, Drug Discov. Today 17 (2012) 1044–1052.
[31] S. Harrisson, P. Couvreur, J. Nicolas, Simple and efficient copper metal-mediated synthesis of alkoxyamine initiators, Polym. Chem. 2 (2011) 1859–1865.
[32] T. Nguyen, M.B. Francis, Practical synthetic route to functionalized rhodamine dyes, Org. Lett. 5 (2003) 3245–3248.
[33] D. Benoit, V. Chaplinski, R. Braslau, C.J. Hawker, Development of a universal alkoxyamine for living free radical polymerizations, J. Am. Chem. Soc. 121 (1999) 3904–3920.
[34] D. Benoit, E. Harth, P. Fox, R.M. Waymouth, C.J. Hawker, Accurate structural control and block formation in the living polymerization of 1,3-dienes by nitroxide-mediated procedures, Macromolecules 33 (2000) 363–370.
[35] K. Matsumoto, T. Iwata, M. Suenaga, Mild oxidation of alcohols using soluble polymer-supported TEMPO in combination with oxone: effect of a basic matrix of TEMPO derivatives, Heterocycles 81 (2010) 2539–2553.
[36] H. Fessi, F. Puisieux, J.P. Devissaguet, N. Ammoury, S. Benita, Nanocapsule formation by interfacial polymer deposition following solvent displacement, Int. J. Pharm. 55 (1989) R1–R4.
[37] J. Nicolas, Y. Guillaneuf, C. Lefay, D. Bertin, D. Gigmes, B. Charleux, Nitroxide-mediated polymerization, Prog. Polym. Sci. 38 (2013) 63–235.
[38] N.J. Turro, G. Lem, I.S. Zavarine, A living free radical exchange reaction for the preparation of photoactive end-labeled monodisperse polymers, Macromolecules 33 (2000) 9782–9785.
[39] O.G. Ballesteros, L. Maretti, R. Sastre, J. Scaiano, Kinetics of cap separation in nitroxide-regulated "living" free radical polymerization: application of a novel methodology involving a prefluorescent nitroxide switch, Macromolecules 34 (2001) 6184–6187.
[40] C.J. Hawker, G.G. Barclay, J. Dao, Radical crossover in nitroxide mediated "living" free radical polymerizations, J. Am. Chem. Soc. 118 (1996) 11467–11471.
[41] S.B. Jhaveri, M. Beinhoff, C.J. Hawker, K.R. Carter, D.Y. Sogah, Chain-end functionalized nanopatterned polymer brushes grown via in situ nitroxide free radical exchange, ACS Nano 2 (2008) 719–727.
[42] H. Wagner, M. Becker, L. Chi, A. Studer, Structuring of polymer brushes and surface nitroxide exchange reactions, Progress in Controlled Radical Polymerization: Materials and Applications, ACS Publications, 2012, pp. 241–256.
[43] J.P. Blinco, K.E. Fairfull-Smith, A.S. Micallef, S.E. Bottle, Highly efficient, stoichiometric radical exchange reactions using isoindoline profluorescent nitroxides, Polym. Chem. 1 (2010) 1009–1012.
[44] Y. Guillaneuf, P.-E. Dufils, L. Autissier, M. Rollet, D. Gigmes, D. Bertin, Radical chain end chemical transformation of SG1-based polystyrenes, Macromolecules 43 (2009) 91–100.
[45] B.H. Lessard, T.P. Bender, Controlled and selective placement of boron subphthalocyanines on either chain end of polymers synthesized by nitroxide mediated polymerization, AIMS Mol. Sci. 2 (2015) 411–426.
[46] C. Cheng, K. Qi, E. Khoshdel, K.L. Wooley, Tandem synthesis of core− shell brush copolymers and their transformation to peripherally cross-linked and hollowed nanostructures, J. Am. Chem. Soc. 128 (2006) 6808–6809.
[47] S.Y. Chen, Y. Huang, R.C.C. Tsiang, Ozonolysis efficiency of PS-b-PI block copolymers for forming nanoporous polystyrene, J. Polym. Sci. A Polym. Chem. 46 (2008) 1964–1973.
[48] S. Sato, Y. Honda, M. Kuwahara, T. Watanabe, Degradation of vulcanized and nonvulcanized polyisoprene rubbers by lipid peroxidation catalyzed by oxidative enzymes and transition metals, Biomacromolecules 4 (2003) 321–329.
[49] K. Rose, A. Steinbüchel, Biodegradation of natural rubber and related compounds: recent insights into a hardly understood catabolic capability of microorganisms, Appl. Environ. Microbiol. 71 (2005) 2803–2812.
[50] H.-C. Yang, J. Silverman, J.J. Wozniak, Low temperature heat shrinkable polymer material, Google Patents, 1986.
[51] L.W. Hertel, G.B. Boder, J.S. Kroin, S.M. Rinzel, G.A. Poore, G.C. Todd, G.B. Grindey, Evaluation of the antitumor activity of gemcitabine (2′, 2′-difluoro-2′-deoxycytidine), Cancer Res. 50 (1990) 4417–4422.
[52] R. Benson, R. Meyer, M. Zaruba, G. McKhann, Cellular autofluorescence—is it due to flavins? J. Histochem. Cytochem. 27 (1979) 44–48.
[53] J.L. Grem, G. Falkson, R.R. Love, D.C. Tormey, A phase II evaluation of combination chemotherapy plus aminoglutethimide in women with metastatic or recurrent breast carcinoma. An Eastern Cooperative Oncology Group Pilot Study, Am. J. Clin. Oncol. 11 (1988) 528–534.
[54] R. Duncan, M. Vicent, F. Greco, R. Nicholson, Polymer–drug conjugates: towards a novel approach for the treatment of endrocine-related cancer, Endocr. Relat. Cancer 12 (2005) S189–S199.
[55] M.J. Vicent, F. Greco, R.I. Nicholson, A. Paul, P.C. Griffiths, R. Duncan, Polymer therapeutics designed for a combination therapy of hormone-dependent cancer, Angew. Chem. 117 (2005) 4129–4134.
[56] F. Greco, M.J. Vicent, S. Gee, A.T. Jones, J. Gee, R.I. Nicholson, R. Duncan, Investigating the mechanism of enhanced cytotoxicity of HPMA copolymer–Dox–AGM in breast cancer cells, J. Control. Release 117 (2007) 28–39.
[57] R.H. Blum, S.K. Carter, Adriamycin: a new anticancer drug with significant clinical activity, Ann. Intern. Med. 80 (1974) 249–259.
[58] S.R. Johnston, M. Dowsett, Aromatase inhibitors for breast cancer: lessons from the laboratory, Nat. Rev. Cancer 3 (2003) 821.
[59] R.J. Santen, T.J. Worgul, E. Samojlik, A. Interrante, A.E. Boucher, A. Lipton, H.A. Harvey, D.S. White, E. Smart, C. Cox, A randomized trial comparing surgical adrenalectomy with aminoglutethimide plus hydrocortisone in women with advanced breast cancer, N. Engl. J. Med. 305 (1981) 545–551.
[60] D. Bertin, F. Chauvin, S. Marque, P. Tordo, Lack of chain length effect on the rate of homolysis of polystyryl-SG1 alkoxyamines, Macromolecules 35 (2002) 3790–3791.
[61] F. Chauvin, P.-E. Dufils, D. Gigmes, Y. Guillaneuf, S.R. Marque, P. Tordo, D. Bertin, Nitroxide-mediated polymerization: the pivotal role of the kd value of the initiating alkoxyamine and the importance of the experimental conditions, Macromolecules 39 (2006) 5238–5250.
[62] G. Audran, P. Brémond, S.R. Marque, G. Obame, Chemically triggered C–ON bond homolysis of alkoxyamines. Part 4: solvent effect, Polym. Chem. 3 (2012) 2901–2908.
[63] G. Moreira, L. Charles, M. Major, F. Vacandio, Y. Guillaneuf, C. Lefay, D. Gigmes, Stability of SG1 nitroxide towards unprotected sugar and lithium salts: a preamble to cellulose modification by nitroxide-mediated graft polymerization, Beilstein J. Org. Chem. 9 (2013) 1589.
[64] P. Xu, E. Gullotti, L. Tong, C.B. Highley, D.R. Errabelli, T. Hasan, J.-X. Cheng, D.S. Kohane, Y. Yeo, Intracellular drug delivery by poly(lactic-co-glycolic acid) nanoparticles, revisited, Mol. Pharm. 6 (2009) 190–201.
[65] C.E. Soma, C. Dubernet, D. Bentolila, S. Benita, P. Couvreur, Reversion of multidrug resistance by co-encapsulation of doxorubicin and cyclosporin A in polyalkylcyanoacrylate nanoparticles, Biomaterials 21 (2000) 1–7.
[66] X. Yang, X. Zhang, Z. Liu, Y. Ma, Y. Huang, Y. Chen, High-efficiency loading and controlled release of doxorubicin hydrochloride on graphene oxide, J. Phys. Chem. C 112 (2008) 17554–17558.
[67] P. Yousefpour, F. Atyabi, E.V. Farahani, R. Sakhtianchi, R. Dinarvand, Polyanionic carbohydrate doxorubicin–dextran nanocomplex as a delivery system for anticancer drugs: in vitro analysis and evaluations, Int. J. Nanomedicine 6 (2011) 1487.
[68] F. Greco, M.J. Vicent, N.A. Penning, R.I. Nicholson, R. Duncan, HPMA

copolymer–aminoglutethimide conjugates inhibit aromatase in MCF-7 cell lines, J. Drug Target. 13 (2005) 459–470.
[69] M. Jarman, A. Foster, P. Goss, L. Griggs, I. Howe, R. Coombes, Metabolism of aminoglutethimide in humans: identification of hydroxylaminoglutethimide as an induced metabolite, Biol. Mass Spectrometry 10 (1983) 620–625.
[70] A.B. Foster, L.J. Griggs, I. Howe, M. Jarman, C.-S. Leung, D. Manson, M.G. Rowlands, Metabolism of aminoglutethimide in humans. Identification of four new urinary metabolites, Drug Metab. Dispos. 12 (1984) 511–516.
[71] F. Julie, G. Mickael, Analysis of drug combinations: current methodological landscape, Pharmacol. Res. Perspect. 3 (2015) e00149.